Magnetic Circular Dichroism of Porphyrin Lanthanide M^{3+} Complexes

VALERY ANDRUSHCHENKO,[1] DANIELE PADULA,[1] ELENA ZHIVOTOVA,[2] SHIGEKI YAMAMOTO,[3] AND PETR BOUŘ[1]*

[1]*Institute of Organic Chemistry and Biochemistry, Academy of Sciences, Prague, Czech Republic*
[2]*Department of Physics, National University of Pharmacy, Ukraine*
[3]*Department of Chemistry, Graduate School of Science, Osaka University, Osaka, Japan*

ABSTRACT Lanthanide complexes exhibit interesting spectroscopic properties yielding many applications as imaging probes, natural chirality amplifiers, and therapeutic agents. However, many properties are not fully understood yet. Therefore, we applied magnetic circular dichroism (MCD) spectroscopy, which provides enhanced information about the underlying electronic structure to a series of lanthanide compounds. The metals in the M^{3+} state included Y, La, Eu, Tb, Dy, Ho, Er, Tm, Yb, and Lu; the spectra were collected for selected tetraphenylporphin (TPP) and octaethylporphin (OEP) complexes in chloroform. While the MCD and UV-VIS absorption spectra were dominated by the porphyrin signal, metal binding significantly modulated them. MCD spectroscopy was found to be better suited to discriminate between various species than absorption spectroscopy alone. The main features and trends in the lanthanide series observed in MCD and absorption spectra of the complexes could be interpreted at the Density Functional Theory (DFT) level, with effective core potentials on metal nuclei. The sum over state (SOS) method was used for simulation of the MCD intensities. The combination of the spectroscopy and quantum-chemical computations is important for understanding the interactions of the metals with the organic compounds. *Chirality 26:655–662, 2014.*

KEY WORDS: magnetic circular dichroism; lanthanides; porphyrin complexes; density functional theory; sum over state computations

INTRODUCTION

Lanthanides include elements with atomic numbers 57–71, and they often occur as M^{3+} ions. Their relatively large size implies both rich coordination chemistry and a wealth of energy levels, thus allowing for numerous applications. Porphyrins[1] and their complexes containing these metals can thus function as light-emitting or absorbing agents, e.g., for biomedical diagnostics.[2] Lanthanides can also be used as quantum dots[3] and the Förster resonance energy transfer (FRET) makes them particularly suitable as fluorescent labels.[4] Their complexes exhibit luminescence under various excitation conditions, even yielding near-IR-emitting materials,[5] and some lanthanide ions were investigated as spectral converters for solar cells.[6] A nice application of bright Eu complexes suitable for mitochondrial imaging was described.[7] Previously, we found that the Raman optical activity (ROA) of simple organic molecules rises by two orders of magnitude when these make a complex with the Eu^{3+} ion,[8] potentially useful in detection of natural molecular chirality and absolute configuration determination.[9]

The diversity of the lanthanides' applications somewhat contrasts with their similar chemical properties. To better understand their electronic structure and chemistry, we took advantage of a relatively complete series of the heavy metals and their complexes with the tetraphenylporphin (TPP) and octaethylporphin (OEP) ligands prepared earlier (Refs. 10 and 11, respectively), and studied them by magnetic circular dichroism (MCD) spectroscopy. Comparison between compounds revealed the potential of MCD spectroscopy to discriminate between rare earth metals and their binding properties. It also provides insight into the properties of the porphyrin ligands, almost universally used in heavy metal chemistry.[12–15]

Although the complexes are not chiral, an external magnetic field perturbs molecular symmetry and induces a difference in absorption of the left- and right-circularly polarized light, i.e., the MCD.[14,16] Compared to unpolarized spectra, such as UV absorption, the differential MCD technique provides positive as well as negative spectral bands. MCD, similar to other chiroptical methods, is generally very sensitive to structure and can thus yield detailed information about studied systems.[17,18] The application span of chiral spectroscopic techniques including MCD has been greatly broadened by the latest introduction of fast and accurate computational techniques allowing one to simulate and interpret the spectra.[19–23]

It is true that in lanthanides the potential of ab initio modeling techniques is rather limited. Relativistic methods necessary to reveal the properties of such heavy elements are currently being developed,[24] but empirical approaches still dominate in descriptions of lanthanide electronic states.[25] Typically, the crystal-field theory is adapted and the metal environment is simulated by a series of empirical parameters.[26–28] As such an approach often lacks predictive capability, chiral spectra can provide an additional motivation to quantum chemists to consider implementation of advanced optical properties at the four-component relativistic level of approximation. In the present study, not directly exploring inner metal electrons, the effective core potentials (ECP)[29,30] within Density Functional Theory (DFT) yielded the basic trends

*Correspondence to: Petr Bouř, Institute of Organic Chemistry and Biochemistry, Academy of Sciences, Flemingovo nám. 2, 166 10 Prague, Czech Republic. E-mail: bour@uochb.cas.cz
Received for publication 4 March 2014; Accepted 15 July 2014
DOI: 10.1002/chir.22365
Published online 13 August 2014 in Wiley Online Library (wileyonlinelibrary.com).

in geometry and spectral properties of the complexes. Note that electronic transitions involving the porphyrin core contribute most to the spectra, i.e., the participation of the metals is limited. The sum-over-state (SOS) theory[22] was used for MCD spectral simulation, as it quickly provides the spectral features with accuracy comparable to the standard coupled-perturbed approaches.[19,21]

As is apparent below, in spite of the chemical similarity, the complexes of individual metals do exhibit different MCD spectra, as the metal bound to porphyrin perturbs the porphyrin electronic system.

EXPERIMENTAL

MCD Measurements

We used TPP and OEP lanthanide acetylacetonate (acac) complexes prepared and described previously[10,11,31] (Fig. 1). MS spectra and results of the elemental analysis can be found in the Supporting Information. For all complexes the molecular ion peak is always present and the MS profile of all complexes is consistent. According to the elemental analysis, however, some complexes exhibit sulfur contents as a residuum from the high-performance liquid chromatography (HPLC) purification process with dimethyl sulfoxide (DMSO), which can thus influence the absolute spectral intensities. According to personal communication with Prof. Saito, residual water may also be present in the compounds.

All samples were dissolved in chloroform. The solvent was purified before each measurement by a standard procedure using an Al_2O_3 column. A nonlanthanide element, Y, was also included, as it exhibits properties similar to lanthanides. All investigated compounds and the concentrations are listed in Supporting Table S1. Spectra of free acacH (acetylacetone, CH_3-CO-CH_2- $COCH_3$) and $TPPH_2$ were measured as well. The signal of acacH, however, was quite weak and reached the UV region only.

The MCD and absorption spectra were measured at room temperature with a Jasco J-815 spectrometer equipped with a 1.5 T permanent magnet. The samples were contained in a rectangular quartz cell of 0.1 cm optical pathlength placed at the middle of the sample compartment. The spectra were recorded for both magnet orientations in the 240–850 nm range, using 0.5 nm resolution, 4 s response time, and a scanning speed of 20 nm/min. Three accumulations were averaged. Finally, solvent spectra acquired at identical conditions were subtracted from those of the samples.

Quantum Chemical Computations

Only the TPP-metal complexes were investigated computationally, as preliminary tests suggested that the OEP complexes behave in a similar way as TPP. To obtain realistic initial geometries, MOPAC[32] software was employed, using the PM7[33] semiempirical method with the SPARKLE[34] representation of the metal. The conformation of the phenyl groups was chosen the same for all compounds, close to the lowest-energy structure of bare TPP molecule (of C_{2h} symmetry, "rlrl" in Ref. 35). Previously, a negligible effect of the porphyrin substituent conformation on the spectra in the visible region was found.[23]

For geometry minimization the BPW91[36] and B3LYP[37] functionals with Pople-type 6-31G** basis set were used within the GAUSSIAN[38] environment. Stuttgart effective core potentials[30] for the metals were used as follows: Y(MWB28), La(MWB46), Eu(MWB52), Tb(MWB54), Dy(MWB55), Ho(MWB56), Er(MWB57), Tm(MWB(58), Yb(MWB59), and Lu(MWB60). For B3LYP, the PCM[39] dielectric model was used to simulate the solvent. For the optimized structures the energy minima were verified by computation of the harmonic vibrational frequencies, which were all positive. Although started from C_1 symmetry, for DFT the complexes usually minimized to structures of C_2 symmetry. In such a case, the higher C_2 symmetry was employed for MCD spectra computations to save computer time.

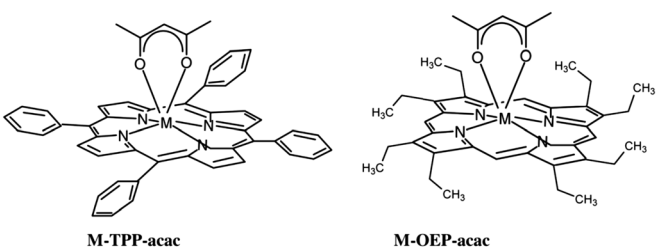

Fig. 1. Studied complexes, M = Y, La, Eu, Tb, Dy, Ho, Er, Tm, Yb and Lu.

The absorption spectra were simulated using GAUSSIAN within the time-dependent density functional theory (TDDFT)[40] at B3LYP/6-31G** level of approximation. Only the results obtained with the PCM solvent correction for chloroform are reported. They are closer to experimental results, although qualitatively the outcome of the vacuum computations was similar. The TDDFT transition energies (not orbital energies!) and wavefunctions obtained by GAUSSIAN were used in our own programs to obtain MCD intensities using the SOS method.[22] The MCD intensities were derived from the "B-terms"[41] computed for each $n \rightarrow j$ transition as:

$$B = \frac{\varepsilon_{\alpha\beta\gamma}}{d_n} \sum_n \mathrm{Im}\left[\sum_{k\neq n} \frac{\langle k|m_\alpha|n\rangle}{E_k - E_n} \langle n|\mu_\beta|j\rangle\langle j|\mu_\gamma|k\rangle + \sum_{k\neq j} \frac{\langle j|m_\alpha|k\rangle}{E_k - E_j} \langle n|\mu_\beta|j\rangle\langle k|\mu_\gamma|n\rangle\right]$$

where $\varepsilon_{\alpha\beta\gamma}$ is the antisymmetric tensor, d_n is the degeneracy of the ground state, E_l is electronic energy of a state l, and m_α and μ_α are the magnetic and electric dipole moment components. Note that this approach allows for A-term computation as well, via an arbitrary perturbation of the degeneracy.[22] Absorption and MCD spectral curves were simulated using Gaussian band shapes 10 nm wide (full width at half maximum).

Within the vertical gradient approximation (VG)[42] possible effects of the vibrational splitting of the lowest-energy electronic transitions (Q-bands) were estimated for the Tb-TPP-acac complex using the FCCLASSES program,[43] working closely with the GAUSSIAN interface.

RESULTS AND DISCUSSION

Calculated Geometries of the TPP Complexes

The metal-oxygen (M-O) and metal-nitrogen (M-N) distances in the M-TPP-acac complexes as obtained by different computational models are summarized in Table S2 and Figure S2. They compare well with available crystal data and previous modeling studies.[44] Both the M-O and M-N distances decrease rather monotonically with the atomic number in the lanthanide series. The PCM solvent environment (chloroform) in combination with the B3LYP/6-31G** approximation level provides a nonsymmetric geometry (C_1) for La, which reflects the large bond lengths and relatively weak complexation affinity of this metal. With the B3LYP/6-31G** method the vacuum distances are shorter than for chloroform, and the difference is on average only slightly larger for M-N (0.003–0.007 Å) than for M-O (0.002–0.004 Å). As apparent from the N-M-N angles (the last two columns in Table S2), with increasing atomic number the angles become wider, i.e., the metal is approaching the porphyrin plane.

Computed Effect of Metal Binding on Porphyrin Spectra

The expected absorption and MCD spectra of the free and complexed porphyrin ligand are summarized in Figure 2, as estimated at the B3LYP/6-31G** approximation level. The vacuum TPP MCD and absorption spectra (top in Fig. 2A) correspond to previous studies.[15,23,45] The addition of the solvent environment (middle, Fig. 2B) significantly modifies the spectra. The wavelengths of the Q-transitions (541 and 579 nm in vacuum) are not much affected (544 and 580 in $CHCl_3$), while the main Soret band shifts more (393 → 401 nm). The intensity changes are larger, the

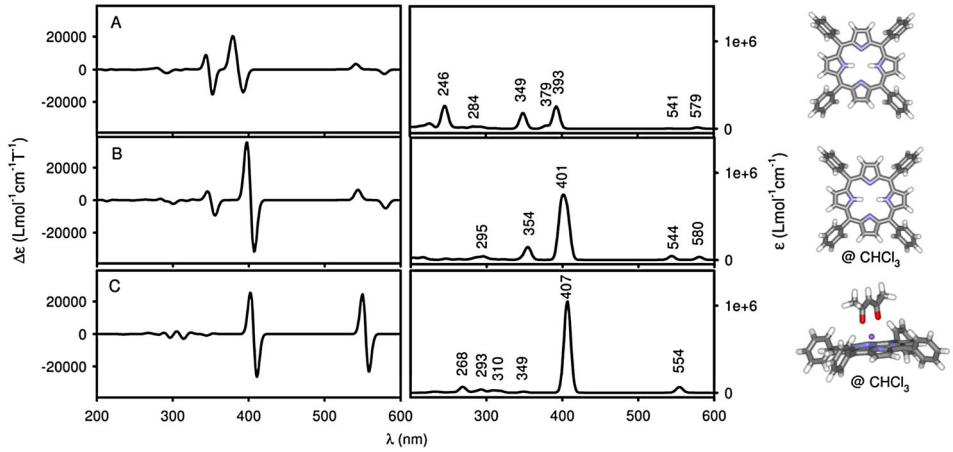

Fig. 2. Computed MCD and absorption spectra (**A**) for free TPP, (**B**) TPP within the PCM($CHCl_3$) environment, and (**C**) Eu- TPP-acac complex.

absorption intensity of the "Q_Y" band (calculated at 544 nm) grows if compared to the Q_X band at 580 nm, and the Soret band grows as well. In MCD spectrum the Soret "-/+" couplet around 400 nm becomes even more dominant, whereas the signal around 349 nm diminishes. The relatively large influence of the environment on MCD intensities was also observed previously, for example, for ZnTPP complexes.[46]

The main simulated TPP spectral features including MCD band signs correspond to the experiment (Refs. 23, 45, and the results below). The fine vibrational Q-bands' splitting[45,47] is not comprised in the electronic model. Experimentally, MCD and absorption spectra of TPP in benzene, for example, exhibit a splitting of the Q_Y band to Q_{Y1} (~510 nm) and Q_{Y0} (550 nm) components, i.e., by 1426 cm^{-1}, and the Q_X splits to Q_{X1} (~590 nm) and Q_{X0} (650 nm, by 1564 cm^{-1}).[45] This correlates with the experimental values of 516 and 551 nm for Q_{Y1} and Q_{Y0}, and 591 and 647 nm for the Q_{X1} and Q_{X0} components for TPP in $CHCl_3$.

The metal complexation of TPP in the Eu-TPP-acac causes weakening of the signal around 350 nm (Fig. 2C) and strengthening of the Soret band at 410 nm. Additionally, the Q-band split is reduced to less than 2 nm, but its MCD intensity increases. The near degeneracy of the electronic states corresponds to the higher effective local symmetry of the porphyrin in the complex, close to the C_4 (or D_{4h} if we neglect the metal) point groups, as opposed to the D_{2h} symmetry of free TPP. Note, however, that the metal is above the porphyrin plane (the out-of-plane deviation is about 1.6 Å for La-TPP-acac, 1.1 Å for Lu-TPP-acac; see also the structure in Fig. 2 and the N-M-N bond angles in Table S2), i.e., far from ideal planar arrangement.

Although the metals do influence the spectra, the strongest transitions within the 200–800 nm region originate almost entirely in the porphyrin aromatic system. The extent to which the metal modifies the LUMO and HOMO TPP orbitals is shown for the Tb-TPP-acac complex in Figure 3. The largest changes between the orbitals in the free and complexed TPP system seem to originate in a lowering of the local TPP symmetry in the complex. Absorption and MCD spectra simulated using other (6-31G, 6-31G*, and 6-31 + G**, see Figure S1) basis sets are very close to those obtained by 6-31G**, which is in accord with our previous results on porphyrin derivatives.[23]

EXPERIMENTAL ABSORPTION AND MCD SPECTRA OF TPP AND OEP COMPLEXES

The experimental spectra of the TPP-acac metal complexes in the Soret and Q regions are plotted in Figure 4. We also plot the MCD/absorption ratio, which enables a better comparison of MCD spectral shapes. The division also partially compensates for a possible experimental error in concentration determination and sample impurities (see Supporting Information). In particular, we suspect that the Eu complexes were prone to decomposition, and might be, for example, contaminated by the free TPP ligand. Note that if decomposition products interfere in the same spectral region, the interference may not be eliminated by the division.

As predicted (Fig. 2), the position of the Soret band of the free porphyrin (Fig. 4) shifts to longer wavelengths (from 418 nm to 412–424 nm in experiment, depending on the metal, 401 – 407 nm in the calculation), and the MCD intensity for the Q transitions (within 500–670 nm) significantly grows upon the metal binding. In experiment, the Q region exhibits a rather complicated vibrational structure; nevertheless, the calculated reduction of the Q-band split in TPP upon metal binding is apparent, as the four strongest bands in TPP are reduced to two in all the complexes.

In the Q-region, all the metals provide very similar absorption and MCD signals. On the other hand, there are clear differences in the Soret region, including absorption and MCD intensities, and, in particular, in MCD band shapes. The positive band at 415 nm in free TPP shifts to ~421 nm in the lanthanide complexes. It is accompanied by a shoulder at 415 nm increasing with the atomic number. Yttrium behaves as Lu in this respect. Rather surprisingly, the increase of absorption intensity is not monotonic with the atomic number in this case. The most absorbing Dy complex has the Soret absorption and MCD about five times larger than for Tm.

The approximate computation based on the relativistic pseudopotentials cannot capture all the fine differences between the metals, in particular the interplay between the inner metal electrons and porphyrin electronic transitions. Nevertheless, as shown in Figure 5, there is a reasonable correlation between the calculated and experimental positions of the absorption bands. Both the Soret and Q transition

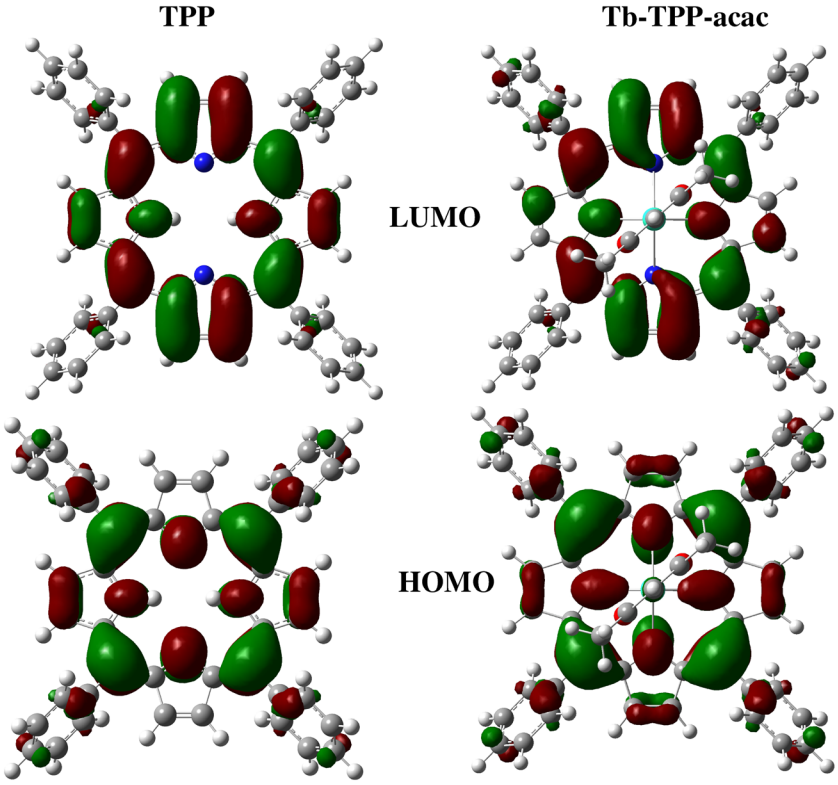

Fig. 3. The HOMO/LUMO orbitals (B3LYP/6-31G**) in the free TPP ligand (left) and the Tb-TPP-acac complex (right).

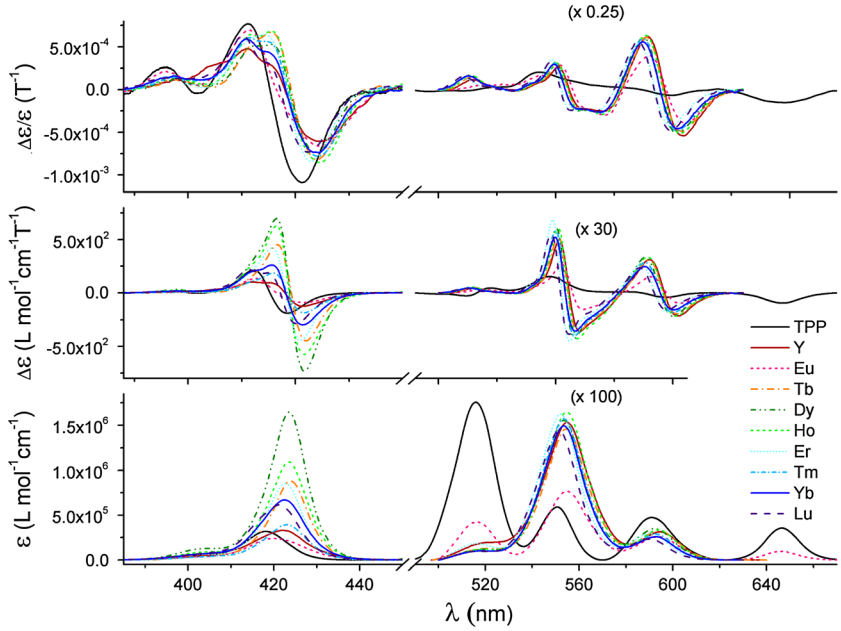

Fig. 4. Experimental absorption (bottom), MCD (middle, ratio MCD/abs at the top) spectra for the TPP-acac metal complexes.

wavelengths decrease with the atomic number, and the B3LYP/PCM/6-31G** computation slightly underestimates the observed changes. The OEP experimental data seem to be closely following the TPP results, except for a relatively large overall shift to shorter wavelength of the Soret (424 nm → 404 nm) and Q (556 nm → 536 nm) transitions, given by the more restricted π-electron conjugation in OEP.

Except for the band shifts, spectra of the OEP complexes are similar to those with the TPP ligand. The absorption and MCD spectra of the OEP-acac complexes are plotted in Figure 6. As for TPP (Fig. 4) the Q-transitions in the OEP complexes are relatively indifferent to the nature of the metal. The Soret band is thus the most sensitive spectral feature in this respect. This is a somewhat counterintuitive finding, as

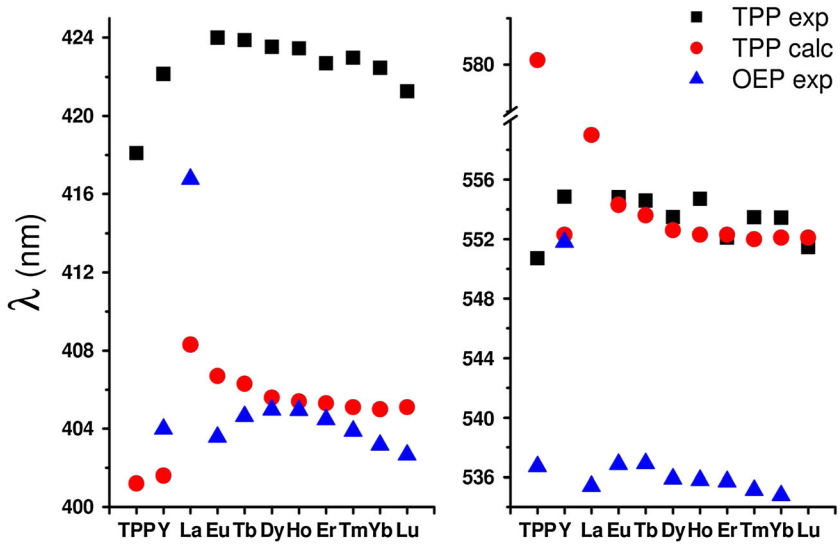

Fig. 5. Calculated and experimental Soret (left) and Q-band (right) positions in the complexes. Note that the experimental wavelengths are affected by the vibronic splitting, not comprised in the theoretical model.

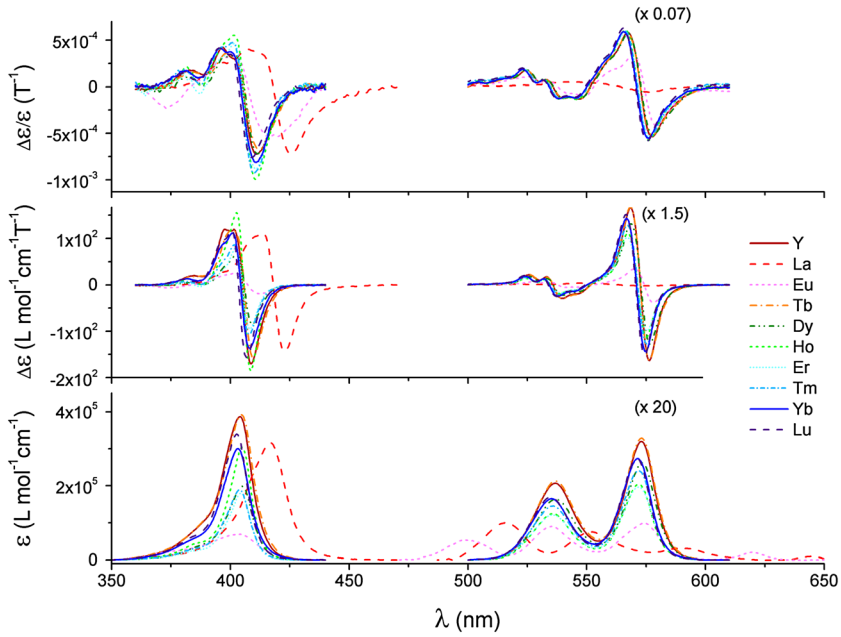

Fig. 6. Experimental absorption and MCD spectra, and the MCD/abs ratio for the OEP-acac metal complexes.

the lowest-energy (highest-wavelength) transitions involving frontier HOMO and LUMO orbitals are usually more sensitive to the molecular environment.

The absorption differences in the Soret bands of the OEP complexes are comparable to TPP. As for TPP, the positive MCD Soret signal splits upon metal binding. However, MCD differences between individual metals appear to be less apparent for OEP than for TPP. Additionally, the highest-wavelength (lowest-energy) absorption and MCD bands of the OEP complexes (around 545 nm) are stronger than the second-highest wavelength one (~530 nm), whereas the relative intensity ratio was found opposite for TPP. After the division, the MCD/absorption ratios (top in Figs. 4 and 6) for TPP and OEP are comparable again.

Lanthanum, available as the La-OEP-acac complex only, provides some outstanding spectral features if compared to the other metals. Its Soret absorption band and corresponding MCD couplet are red-shifted to 417 nm, compared to 403–405 nm observed for the other metals (Fig. 6). This as also predicted by the computation, albeit for the La-TPP-acac complex and to a lesser extent (Fig. 5). Its absorption spectral pattern in the Q region is also different in that, instead of the two intense bands visible for the other complexes (~536/572 nm), four bands appear at 516, 552, 589, and 645 nm. The MCD signal is very weak compared to the other metals. The richer Q signal splitting can be deduced from the lowering of the symmetry of the La complex (cf. Table S2), although we cannot currently explain the experimental intensity pattern in detail.

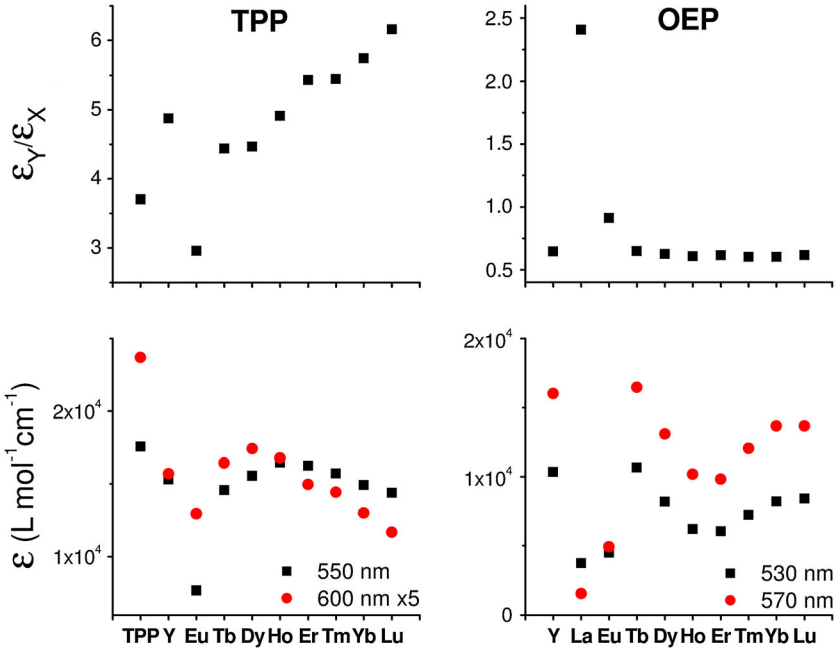

Fig. 7. Experimental absorption intensity ratios ($\varepsilon_{550}/\varepsilon_{600}$ for TPP and $\varepsilon_{530}/\varepsilon_{570}$ for OEP), and absolute intensities (ε) of the Q-bands in M-TPP-acac and M-OEP-acac complexes.

Apart from the Soret and Q, we acquired the absorption and MCD spectra also in the UV region (~200–400 nm, Fig. S3). Similarly as for the two other regions, the UV transitions are also sensitive to metal binding, but they do not appear to be too sensitive to a particular metal type. Additionally, the signal here is rather weak and prone to artifacts due to strong solvent absorption. In general, however, the MCD features are quite reproducible everywhere, e.g., different magnet orientation providing nearly mirror-image spectra, as documented for the Dy complexes in Figure S4.

In Figure 7, selected experimental spectral intensity features for the Q bands are plotted as compared for different metals. We did not find any similar correlations for the Soret band. This is in agreement with the computations (Tables S3 and S4) providing for only minimal differences for the different metals. For Q, however, the ratio of the two strongest absorption bands seems to monotonically increase/decrease with the atomic number for the TPP/OEP complexes. On the other hand, the integrated absorption intensity has an extreme around Z = 65-67 (Tb, Dy, Ho). From the dependencies, we can deduce that the atomic number plays a dominant role for the complexes' spectroscopic properties, although many factors can contribute. For example, lanthanides with a higher atomic number bind stronger to the porphyrin and acac ligands (Table S2). Also the differences in atomic mass contribute to a different vibrational splitting determining the fine intensity pattern, especially for the Q transitions.

Vibrational Splitting of the Q Transitions

Finally, at least at a qualitative level, we attempted to obtain an insight into the vibrational splitting of the Q transitions in the TbTPPacac complex. A full interpretation of the vibronic pattern is associated with many problems and requires inclusion of the Herzberg-Teller[51] and Duschinsky[52] effects relying on a complete harmonic description of the excited state potential energy surface.[42] Different contributions to the vibrational splitting of the Q bands were analyzed in

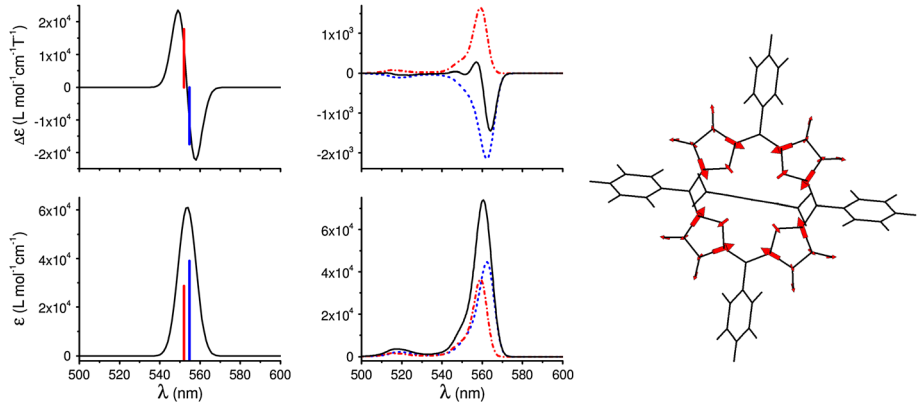

Fig. 8. Calculated absorption and MCD spectra of the Tb-TPP-acac without (left) and with (middle) the vibrational structure for the two (red and blue) Q electronic transitions; the resultant spectra are plotted by the black line. The normal mode displacement for the 1371 cm^{-1} transition most contributing to the splitting is indicated at the right-hand side.

detail for the bare porphyrin moiety in Ref. 48. With respect to the unsubstituted porphyrin analyzed therein, our vibronic broadening is slightly larger due to vibronic transitions associated with low frequencies. These are more numerous because of the presence of the four phenyl moieties in our molecule.

As is apparent from the calculated MCD spectra plotted in Figure 8, the VG approach provides the basic split feature observed in the experiment: the two electronic transitions provide opposite MCD signs. Each state splits into two vibronic bands. The vibronic progression is characterized by a spacing between the two bands (518 and 559 nm) of about 1415 cm^{-1}. The two states give negative (state 1) and positive (state 2) components of a MCD couplet. This roughly corresponds to the observation, although the intensity of the lower-wavenumber band (~518 nm) is strongly underestimated by the calculation (cf. Fig. 4). A more detailed analysis of the vibrational progression reveals that characteristic normal modes contributing most to the intensities largely involve C = C and M-N stretching with frequencies of 1371 (displayed in Fig. 8), 1537, and 1581 cm^{-1}. All of them belong to A irreducible representation.

A more precise vibronic MCD model would have to include the coupling between the two involved electronic excited states, which are nearly degenerate (555 and 552 nm). Currently, however, vibronic MCD calculation is possible only for pure B-terms.[49] In the future, time-dependent approaches taking into account coupling between excited states may provide a better description.[50] The progress of the MCD interpretation technique can thus have a direct impact on discrimination of the fine binding properties of the lanthanide and rare earth metals.

CONCLUSIONS

We investigated MCD of a series of the porphyrin complexes in order to estimate the potential of this spectroscopy for analytical and spectroscopic studies of lanthanides and other rare-earth elements and their interactions with organic compounds. In spite of the structural similarity, specific MCD and absorption features were observed for individual metals as modifications of the porphyrin signal in the complexes. The main trends observed in the spectra could be interpreted on the basis of the DFT computations. In the lanthanide series (i.e., except for yttrium) many properties strongly correlated with the atomic number. However, finer spectral differences suggest a more complicated progression of the electronic structure than a linear dependence. The TPP and OEP ligands behaved similarly, with the largest differences in the Q region.

The vibronic theory available only recently provided a reasonable understanding of the fine vibrational splitting observed in the Q-branch. Overall, we find that the MCD technique is a useful supplement of the absorption spectroscopy. In spectroscopy and analytical chemistry of lanthanides, differences in MCD spectral shapes can enhance resolution of the metals and contribute to an understanding of their structure and binding properties.

ACKNOWLEDGMENTS

Supported by the Academy of Sciences (M200550902), Grant Agency of the Czech Republic (13-03978S and P208/11/0105), and Ministry of Education (LH11033). We thank Petr Štěpánek for the help with the measurements.

SUPPORTING INFORMATION

Additional supporting information may be found in the online version of this article at the publisher's web-site.

LITERATURE CITED

1. Kessel D, Cheng ML. Biological and biophysical properties of the tumor-localizing component of hematoporphyrin derivative. Cancer Res 1985; 45(7):3053–3057.
2. Sigel A, Sigel H, editors. Metal ions in biological systems, Vol. 42. New York: Marcel Dekker; 2004.
3. Geißler D, Linden S, Liermann K, Wegner KD, Charbonnière LC, Hildebrandt N. Lanthanides and quantum dots as forster resonance energy transfer agents for diagnostics and cellular imaging. Inorg Chem 2013;53(4):1824–1838.
4. Handle HL, Gillies RJ. Lanthanide-based luminescent assays for ligand-receptor interactions. Life Sci 2005;77:361–371.
5. Bünzli JCG, Piguet C. Taking advantage of luminescent lanthanide ions. Chem Soc Rev 2005;34:1048–1077.
6. van der Ende BM, Aartsa L, Meijerink A. Lanthanide ions as spectral converters for solar cells. Phys Chem Chem Phys 2009;11:11081–11095.
7. Walton JW, Bourdolle A, Butler SJ, Soulie M, Delbianco M, McMahon BK, Pal R, Puschmann H, Zwier JM, Lamarque L, Maury O, Andraudb C, Parker D. Very bright europium complexes that stain cellular mitochondria. Chem Commun 2013;49:1600–1602.
8. Yamamoto S, Bouř P. Detection of molecular chirality by induced resonance Raman optical activity in europium complexes. Angew Chem Int Ed 2012;51(44):11058–11061.
9. Yamamoto S, Bouř P. Transition polarizability model of induced resonance Raman optical activity. J Comput Chem 2013;34:2152–2158.
10. Saitoh K, Shibata Y, Suzuki N. Factors influencing the retention of rare earth-tetraphenylporphine complexes in reversed-phashe high-performance liquid chromatography. J Chromatogr 1991;542:351–363.
11. Shibata Y, Saitoh K, Suzuki N. Control of the retention selectivity of rare earth octaethylporphyrins in reversed-phase high-performance liquid chromatography using amines as mobile phase additives. J Chromatogr 1992;598:73–79.
12. Huang X, Nakanishi K, Berova N. Porphyrins and metalloporphyrins: versatile circular dichroic reporter groups for structural studies. Chirality 2000;12:237–255.
13. Gouterman M. Spectra of porphyrins. J Mol Spectrosc 1961;6:138–163.
14. Barron LD. Molecular light scattering and optical activity. Cambridge, UK: Cambridge University Press; 2004.
15. Mason WR. A practical guide to magnetic circular dichroism spectroscopy. Portland, OR: Wiley-Interscience; 2007.
16. Stephens PJ. Magnetic circular dichroism. Annu Rev Phys Chem 1974;25:201–232.
17. Barron LD, Hecht L, McColl IH, Blanch EW. Raman optical activity comes of age. Mol Phys 2004;102(8):731–744.
18. Nafie L. Vibrational optical activity: Principles and applications. Chichester, UK: Wiley; 2011.
19. Seth M, Krykunov M, Ziegler T, Autschbach J, Banerjee A. Application of magnetically perturbed time-dependent density functional theory to magnetic circular dichroism: Calculation of B terms. J Chem Phys 2008;128(14):144105.
20. Seth M, Krykunov M, Ziegler T, Autschbach J. Application of magnetically perturbed time-dependent density functional theory to magnetic circular dichroism. II. Calculation of A terms. J Chem Phys 2008;128 (23):234102.
21. Solheim H, Ruud K, Coriani S, Norman P. Complex polarization propagator calculations of magnetic circular dichroism spectra. J Chem Phys 2008;128:094103.
22. Štpánek P, Bouř P. Computation of magnetic circular dichroism by sum over states summations. J Comput Chem 2013;34:1531–1539.
23. Štpánek P, Andrushchenko V, Ruud K, Bouř P. Porphyrin protonation studied by magnetic circular dichroism. J Phys Chem A 2012;116(1):778–783.
24. Wodynski A, Repisky M, Pecul M. A comparison of two-component and four-component approaches for calculations of spin-spin coupling constants and NMR shielding constants of transition metal cyanides. J Chem Phys 2012;137:014311.

25. Dorenbos P. A review on how lanthanide impurity levels change with chemistry and structure of inorganic compounds. ECS J Solid State Sci Technol 2013;2(2):R3001–R3011.
26. Dieke GH, Crosswhite HM. The spectra of the doubly and triply ionized rare earths. Appl Optics 1963;2(7):675–686.
27. Varsanyi F, Dieke GH. Energy levels of hexagonal ErCl3. J Chem Phys 1962;36(11):2951–2961.
28. Racah G. Theory of complex spectra. IV Phys Rev 1949;76(9):1352–1365.
29. Hay PJ, Wadt WR. Ab initio effective core potentials for molecular calculations. Potentials for K to Au including the outermost core orbitals. J Chem Phys 1985;82:299–310.
30. Dolg M. Relativistic electronic structure theory. In: Schwerdtfeger P, editor. Part 1: Fundamentals, theoretical and computational chemistry. Amsterdam: Elsevier; 2002. p 793–862.
31. Suzuki N, Saitoh K, Shibata Y. High-performance thin-layer chromatography of rare earth tetraphenylporphine complexes. J Chromatogr A 1990;504:179–185.
32. Steward JJP. MOPAC2009. http://openmopac.net/. Colorado Springs, CO: Steward Computational Chemistry; 2008.
33. Stewart JJP. Optimization of parameters for semiempirical methods. VI: More modifications to the NDDO approximations and re-optimization of parameters. J Mol Model 2013;19:1–32.
34. Dutra JDL, Filho MAM, Rocha GB, Freire RO, Simas AM, Stewart JJP. Sparkle/PM7 lanthanide parameters for the modeling of complexes and materials. J Chem Theor Comput 2013;9(8):3333–3341.
35. Setnička V, Urbanová M, Bouř P, Král V, Volka K. Vibrational circular dichroism of 1,1-binaphthyl derivatives: experimental and theoretical study. J Phys Chem A 2001;105:8931–8938.
36. Becke A. Density-functional exchange-energy approximation with correct asymptotic behavior. Phys Rev A 1988;38:3098–3100.
37. Becke AD. Density-functional thermochemistry. III. The role of exact exchange. J Chem Phys 1993;98:5648–5652.
38. Frisch MJ, Trucks GW, Schlegel HB, Scuseria GE, Robb MA, Cheeseman JR, Scalmani G, Barone V, Mennucci B, Petersson GA, Nakatsuji H, Caricato M, Li X, Hratchian HP, Izmaylov AF, Bloino J, Zheng G, Sonnenberg JL, Hada M, Ehara M, Toyota K, Fukuda R, Hasegawa J, Ishida M, Nakajima T, Honda Y, Kitao O, Nakai H, Vreven T, Montgomery JJA, Peralta JE, Ogliaro F, Bearpark M, Heyd JJ, Brothers E, Kudin KN, Staroverov VN, Kobayashi R, Normand J, Raghavachari K, Rendell A, Burant JC, Iyengar SS, Tomasi J, Cossi M, Rega N, Millam JM, Klene M, Knox JE, Cross JB, Bakken V, Adamo C, Jaramillo J, Gomperts R, Stratmann RE, Yazyev O, Austin AJ, Cammi R, Pomelli C, Ochterski JW, Martin RL, Morokuma K, Zakrzewski VG, Voth GA, Salvador P, Dannenberg JJ, Dapprich S, Daniels AD, Farkas O, Foresman JB, Ortiz JV, Cioslowski J, Fox DJ. Gaussian 09, Revision D01. Wallingford, CT: Gaussian, Inc.; 2009.
39. Mennucci B, Cappelli C, Cammi R, Tomasi J. Modeling solvent effects on chiroptical properties. Chirality 2011;23(9):717–729.
40. Furche F, Ahlrichs R. Adiabatic time-dependent density functional methods for excited state properties. J Chem Phys 2002;116(6):7433–7447.
41. Stephens PJ. Theory of magnetic circular dichroism. J Chem Phys 1970; 52(7):3489–3516.
42. Ferrer FJA, Santoro F. Comparison of vertical and adiabatic harmonic approaches for the calculation of the vibrational structure of electronic spectra. Phys Chem Chem Phys 2012;14:13549–13563.
43. Santoro F. FCclasses. 2.1. Pisa, Italy: Istituto per i Processi Chimico-Fisici - CNR; 2012.
44. Ferguson DM, Raber DJ. Molecular mechanics calculations of several lanthanide complexes: an application of the random incremental pulse search. J Comput Chem 1990;11(9):1061–1071.
45. Sutherland JC. The magnetic optical activity of porphyrins. In: Dolphin D, editor. The porphyrins, Vol. III. New York: Academic Press; 1978. p 225–248.
46. Kintner ET, Nardo JV, Dawson JH. Magnetic circular dichroism spectroscopy of zinc(II) tetraphenylporphyrin-ligand complexes: the effect of the axial ligand on spectral properties. Spectrochim Acta A 1994; 50(3):493–507.
47. Stradomska A, Knoester J. Shape of the Q band in the absorption spectra of porphyrin nanotubes: Vibronic coupling or exciton effects? J Chem Phys 2010;133:094701.
48. Santoro F, Lami A, Improta R, Bloino J, Barone V. Effective method for the computation of optical spectra of large molecules at finite temperature including the Duschinsky and Herzberg–Teller effect: The Q_x band of porphyrin as a case study. J Chem Phys 2008;128 (22):224311.
49. Lin N, Solheim H, Zhao X, Santoro F, Ruud K. First principles studies of the vibrationally resolved magnetic circular dichroism spectra of biphenylene. J Chem Theory Comput 2013;9:1557–1567.
50. Padula D, Picconi D, Lami A, Pescitelli G, Santoro F. Electronic circular dichroism in exciton-coupled dimers: vibronic spectra from a general all-coordinates quantum-dynamical approach. J Phys Chem A 2013;117:3355–3368.
51. Herzberg G, Teller E. Schwingungsstruktur der Elektronenubergange bei mehratomigen Molekulen. Z Phys Chem (Leipzig) 1933; B21:410–446.
52. Duschinsky F. On the interpretation of electronic spectra of polyatomic molecules. Acta Physicochim URSS 1937;1937(7).